Chemical Science

EDGE ARTICLE

View Article Online
View Journal | View Issue

Cite this: *Chem. Sci.*, 2016, **7**, 5805

Solid solution of a zeolite and a framework-bound OSDA-containing molecular sieve†

Jun Kyu Lee, Jeong Hwan Lee, Nak Ho Ahn, Kwang Ho Cho and Suk Bong Hong*

Received 12th May 2016
Accepted 19th May 2016

DOI: 10.1039/c6sc02092e

www.rsc.org/chemicalscience

The structure of the as-made, hydrated form of ECR-40C, synthesized in the presence of (2-hydroxyethyl) trimethylammonium ($HTMA^+$) ions as an organic structure-directing agent (OSDA) and 2 wt% (relative to alumina in the synthesis mixture) of aluminosilicate zeolite UZM-22 with the MEI topology as seeds, has been determined using synchrotron powder X-ray diffraction and Rietveld analyses. Two different types of organic species were suggested to exist in ECR-40C: the encapsulated $HTMA^+$ ions with one intramolecular C–H···O hydrogen bond, typical of OSDA molecules in as-made UZM-22, and the framework-bound cations. A combination of elemental and thermal analyses, Na^+ ion exchange, and multinuclear MAS NMR and IR spectroscopies clearly shows the coexistence of the zeolite and framework-bound OSDA-containing molecular sieve (FOMS) domains with a proportion of approximately 3 : 2 in ECR-40C crystals. TEM elemental mapping reveals that the Na^+ ions exchanged with the $HTMA^+$ ions into as-made ECR-40C are uniformly distributed throughout the ECR-40C crystals. Therefore, ECR-40C is not a pure FOMS but a solid solution of a zeolite and a FOMS (*i.e.*, UZM-22 and ECR-40-type FOMS), which has never been recognized or addressed before. The overall characterization results of this work demonstrate that the proportion of the zeolite domain in such solid-solutions varies significantly with the number of OH groups in OSDAs.

Introduction

Zeolites and molecular sieves are widely used in a variety of commercial applications as catalysts and separation media.[1,2] To further improve their functional properties for expanded use, considerable efforts have been devoted over more than a decade to the synthesis of inorganic–organic hybrid materials with organic moieties incorporated into the inorganic framework.[3] Indeed, if successful, new organic functionalities with tunable geometrical features can be introduced as catalytic and/or adsorption sites into the void spaces of this important class of crystalline, microporous materials. In many cases, on the other hand, the synthesis of such hybrid solids includes the use of organosilicon compounds, the Si atoms of which are incorporated as tetrahedral atoms (T-atoms) in their inorganic framework. For example, organosilanes containing organic functional groups and alkylammonium-bound organosilanes have been used as a (partial) silica source and an organic structure-directing agent (OSDA) in the synthesis of inorganic–organic hybrid molecular sieves, respectively.[4–8] However, the organic contents (<10 wt%) in all final crystalline structures, except for organoaluminosilicate ECS materials,[7,8] are not so large, mainly due to the instability of Si–C bonds in hydrothermal synthesis conditions.

Very recently, we have demonstrated that ECR-40, first reported as a silicoaluminophosphate (SAPO) molecular sieve with the MEI topology in 1999,[9,10] is a family of inorganic–organic hybrid networks in which the OSDA molecules used in their synthesis are covalently bonded to the inorganic framework, *i.e.*, framework-bound OSDA-containing molecular sieves (FOMSs).[11] In our preliminary communication, for that reason, the two ECR-40 materials synthesized using tris(2-hydroxyethyl)methylammonium ($THMA^+$) and bis(2-hydroxyethyl)dimethylammonium ($BHDMA^+$) ions, the OSDAs described in the original Exxon patent on this hybrid phase (Fig. 1),[9] have been referred to as ECR-40A and ECR-40B, respectively. We were also able to synthesize three new members of the ECR-40 family of FOMSs, denoted as ECR-40C, ECR-40D and ECR-40E, using (2-hydroxyethyl)-trimethylammonium ($HTMA^+$), bis(2-hydroxyethyl)methylamine (BHMA) and bis(2-hydroxyethyl)ethylamine (BHEA) as their respective OSDAs with the aid of a seeding technique (Table 1). The ECR-40 family is notably different from the already known FOMSs, such as the azamacrocycle-containing gallophosphate and ethylenediamine-containing germanate (SU-77) crystallized in the presence of F^- ions,[12,13] because the inorganic part is a truly zeolite 3D (4,2)-net. It is worth noting that the OSDA used in the synthesis of the ECR-40 family may contain three ($THMA^+$), two ($BHDMA^+$, BHMA and BHEA) or one ($HTMA^+$) OH groups available for covalent bonding to the inorganic framework.

Center for Ordered Nanoporous Materials Synthesis, School of Environmental Science and Engineering, POSTECH, Pohang 790-784, Korea. E-mail: sbhong@postech.ac.kr

† Electronic supplementary information (ESI) available. See DOI: 10.1039/c6sc02092e

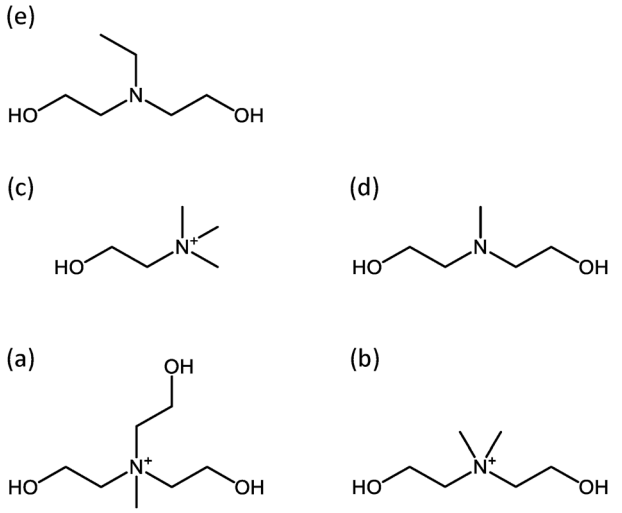

Fig. 1 Alkanolammonium ions and alkanolamines employed as OSDAs in this work: (a) tris(2-hydroxyethyl)methylammonium ($THMA^+$), (b) bis(2-hydroxyethyl)dimethylammonium ($BHDMA^+$), (c) (2-hydroxyethyl)trimethylammonium ($HTMA^+$), (d) bis(2-hydroxyethyl) methylamine (BHMA) and (e) bis(2-hydroxyethyl)ethylamine (BHEA).

In the present study we show that several members of the ECR-40 family stated above are solid solutions of a zeolite and a FOMS rather than pure FOMS. This is partially in contrast to our recent paper,[11] in which the possibility of such a new type of zeolite–FOMS solid-solution was not considered. In fact, the framework structures of the ECR-40 family of FOMSs determined using synchrotron powder X-ray diffraction (XRD) and Rietveld analyses were essentially identical with the MEI zeolite structure, except differences (6 *vs.* 4) in the coordination number of the apex framework atoms of their 13-hedral $[3^14^65^6]$ building units. Moreover, the relative proportions of the zeolite domain in most ECR-40-type FOMSs were found to be ≤20% so that its existence could not be easily detected by powder XRD and Rietveld analyses. Here we have also analyzed a series of mother-liquors and solid products separated as a function of time during the crystallization of ECR-40C, which has the largest zeolite portion (~60%) among the members of the ECR-40 family, using various characterization methods in order to understand the crystallization mechanism of zeolite–FOMS solid solutions. While framework-bound OSDAs impair the microporosity, on the other hand, they can give a new function or surface selectivity to such a family of hybrid materials. For example, alkylamines are commonly used not only as OSDAs in zeolite synthesis, but also as CO_2 adsorbents in the liquid phase.[14] Thus, once these organic species are directly bonded to the zeolite framework without protonation, the resulting zeolite–FOMS solid solutions, the microporosity of which cannot be lower than that of pure FOMSs, may be potentially useful for selective CO_2 adsorption.

Experimental section

Synthesis and cation exchange

Five members of the ECR-40 family were synthesized according to the procedures described in our recent work.[11] Three of the germanoaluminophosphate (GeAPO) versions, namely, the PST-10 family of FOMSs, were synthesized by substituting germanium oxide for colloidal silica in the synthesis mixtures containing $THMA^+$, $BHDMA^+$ and $HTMA^+$ ions as OSDAs, respectively. Aluminosilicate zeolite UZM-22 with the MEI topology (Si/Al = 4.7) was synthesized in the mixed Li^+–Sr^{2+}–$HTMA^+$ structure-directing agent system following the

Table 1 SAPO and GeAPO phases obtained using various alkanolammonium ions and alkanolamines as OSDAs.[a] Adapted from ref. 11

Run	Seeds[b]	Crystallization time (days)	R[c]	Product[d]	
				Me = Si	Me = Ge
1	—	12	THMAOH	ECR-40A	GeAPO-5 + L
2	UZM-22	12	THMAOH	ECR-40A	L + (PST-10A)
3	ECR-40A	12	THMAOH	ECR-40A	PST-10A
4	—	24	BHDMAOH	PB + L	PB
5	UZM-22	12	BHDMAOH	ECR-40B	L + (PST-10B)
6	ECR-40A	12	BHDMAOH	ECR-40B	PST-10B
7	—	24	HTMAOH	PB + L	PB
8[e]	UZM-22	16	HTMAOH	ECR-40C	L + PST-10C
9	ECR-40A	16	HTMAOH	ECR-40C + PB	PST-10C
10	—	24	BHMA	ECR-40D + SAPO-34	PB
11	UZM-22	12	BHMA	ECR-40D	PB
12	ECR-40A	12	BHMA	ECR-40D	PST-10D + PB + (GeAPO-34)
13	—	24	BHEA	L + SAPO-34 + PB	PB
14	UZM-22	12	BHEA	ECR-40E	PB
15	ECR-40A	12	BHEA	ECR-40E	L + PST-10E + PB

[a] The composition of the synthesis mixture was $2.0R : 1.0Al_2O_3 : 0.75P_2O_5 : 0.75MeO_2 : 80H_2O$. SAPO and GeAPO FOMS syntheses were performed under rotation (60 rpm) at 160 and 140 °C, respectively, unless otherwise stated. [b] If required, 2 wt% (of the alumina in the synthesis mixture) as-made UZM-22 or ECR-40A crystals were added as seeds. [c] The same abbreviations as those in Fig. 1. [d] The product appearing first is the major phase, and that obtained in a trace amount is given in parentheses; L and PB are layered phase and pseudoboehmite, the alumina starting material, respectively. [e] Performed at 140 °C.

procedure given elsewhere.[15,16] All the materials prepared here are highly crystalline and no X-ray reflections other than those from the MEI structure[17] are observed (Fig. S1, ESI†). For comparison, boehmite was obtained from Poshial.

To investigate the formation pathway for ECR-40C crystals, a synthesis mixture with the composition $2.0HTMAOH : 1.0Al_2O_3 : 0.75P_2O_5 : 0.75SiO_2 : 80H_2O$ was prepared. A small amount (2 wt% of the alumina in the SAPO gel) of as-made UZM-22 was added to this synthesis mixture and stirred overnight at room temperature. Then, the solid and solution parts of the final synthesis mixture were separated by centrifugation (15 000 rpm, 10 min). The recovered solid was redispersed in deionized water using an ultrasonic bath (100 W, 42 kHz) for 1 h with subsequent centrifugation, which was repeated three times. Finally, the resulting solid was dried overnight at room temperature. The synthesis mixture prepared above was also subjected to crystallization of ECR-40C within Teflon-lined 23 mL autoclaves under rotation (60 rpm) at 140 °C for a total period of 20 days. During the crystallization, the solid products and mother-liquors were periodically separated by centrifugation.

Na^+, $THMA^+$, $BHDMA^+$ and $HTMA^+$ ion exchanges were performed using 1.0 M solutions (1.0 g solid per 100 mL solution) of $NaNO_3$ and iodide salt of the corresponding OSDA cations at 80 °C for 4 h.

Characterization

Powder XRD, elemental and thermal analyses, and multinuclear solution and solid-state NMR measurements were carried out as described elsewhere.[11] The relative crystallinities of a series of solid products recovered at different time intervals during ECR-40C crystallization were determined by comparing the area of the intense X-ray peak around $2\theta = 23.5°$, corresponding to the (122) reflection of the MEI structure, with that of a fully crystallized ECR-40C sample obtained after 20 days at 140 °C. The yield of each product was calculated by dividing the weight of the product obtained after crystallization for a given time by the total weight of the oxide forms of all of the components in the synthesis mixture except water.

High-resolution transmission electron microscopy images with energy-dispersive X-ray chemical mapping were obtained with an omega-filter-equipped JEOL JEM-2200FS transmission electron microscope (TEM) operated at 200 kV. The IR spectra in the C–H and O–H stretching regions were measured on a Midac M2000 FT-IR spectrometer using self-supporting zeolite wafers. Prior to IR experiments, the zeolite wafers were dehydrated under vacuum to a residual pressure of 10^{-3} Torr overnight at 200 °C inside a home-built IR cell with CaF_2 windows. Then, the IR spectra were recorded under flowing N_2 at different temperatures. Typically, 256 scans were accumulated.

Structural analysis

For detailed structural analyses of the as-made, hydrated forms of ECR-40C and PST-10C, powder synchrotron diffraction data were collected on the 9B beamline equipped with a ceramic furnace of the Pohang Acceleration Laboratory (PAL), Pohang, using monochromated X-rays ($\lambda = 1.5475$ Å). The detector arm of the vertical scan diffractometer consists of seven sets of Soller slits, flat Ge(111) crystal analyzers, anti-scatter baffles, and scintillation detectors, with each set separated by 20°. Data were obtained on the sample at room temperature in flat plate mode, with a step size of 0.01° and an overlap of 0.5° to the next detector bank over the 2θ range of 5.0–100.0 or 6.0–90°. Initial structure models were determined by the dual-space method using the FOCUS[18] and powder charge flipping (pCF) algorithms.[19] The structures were then refined *via* the Rietveld method using the GSAS suite of programs and EXPGUI graphical interface.[20–22] ECR-40C and PST-10C were modelled as pure-silica and GeAPO frameworks, respectively. The framework Al–O, P–O, Si–O, Ge–O and O–O(Si) distances were soft constrained to 1.73 Å ($\sigma = 0.01$ Å), 1.51 Å ($\sigma = 0.01$ Å), 1.62 Å ($\sigma = 0.01$ Å), 1.80 Å ($\sigma = 0.01$ Å) and 2.65 Å ($\sigma = 0.01$ Å), respectively. The Al–O_R distance, where O_R is O atoms in the OSDA molecule, as well as O_R–O_R one, was not restrained. Peak shape was modelled using the pseudo-Voigt profile function.[23] The isotropic atomic displacement parameters of the framework atoms were constrained in groups for the tetrahedral sites (Al, P, Si and Ge) and O atoms, respectively. The OSDA molecules were included as a rigid-body, and their locations and orientations were optimized using the parallel tempering method implemented in the FOX program.[24] The rigid bodies were restrained by interatomic distance and angle restraints and were allowed to translate and rotate as a whole. The positions of water molecules were derived from Fourier difference maps. The convergence was achieved by refining simultaneously all profile parameters, scale factor, lattice constants, 2θ zero-point, atomic positional and thermal displacement parameters, and occupancy factors for the framework atoms and water O atoms. The data collection and crystallographic parameters are summarized in Table S1, ESI.†

Results and discussion

Structural details

We begin the discussion by referring to our recent syntheses on the ECR-40 and PST-10 families of FOMSs with SAPO and GeAPO compositions, respectively, as these data have triggered the present study. The crystallization of ECR-40B, ECR-40D and ECR-40E, unlike the case of ECR-40A (synthesized using $THMA^+$ ions, with three OH groups, without seeding), includes the use of 2 wt% (relative to alumina in the SAPO gel) of either as-made ECR-40A or UZM-22 crystals as seeds, as well as an OSDA species containing two OH groups. However, we were not able to obtain ECR-40C in its pure form using ECR-40A as seeds in the presence of $HTMA^+$, with one OH group as an OSDA. As shown in Table 1, the synthesis of pure ECR-40C was possible only when UZM-22 was used as seeds. This suggests that the ability of the aluminosilicate zeolite UZM-22 to induce the crystallization of ECR-40C is stronger than that of the SAPO FOMS ECR-40A. We should note here that while the Si/(Si + Al + P) ratio (0.29) of ECR-40C, determined by elemental analysis, is considerably larger than the ratio (0.20) of ECR-40A, the opposite holds for their solid yield (11 *vs.* 44%).[11] It thus appears that a more significant amount of Si is required for the crystallization of the

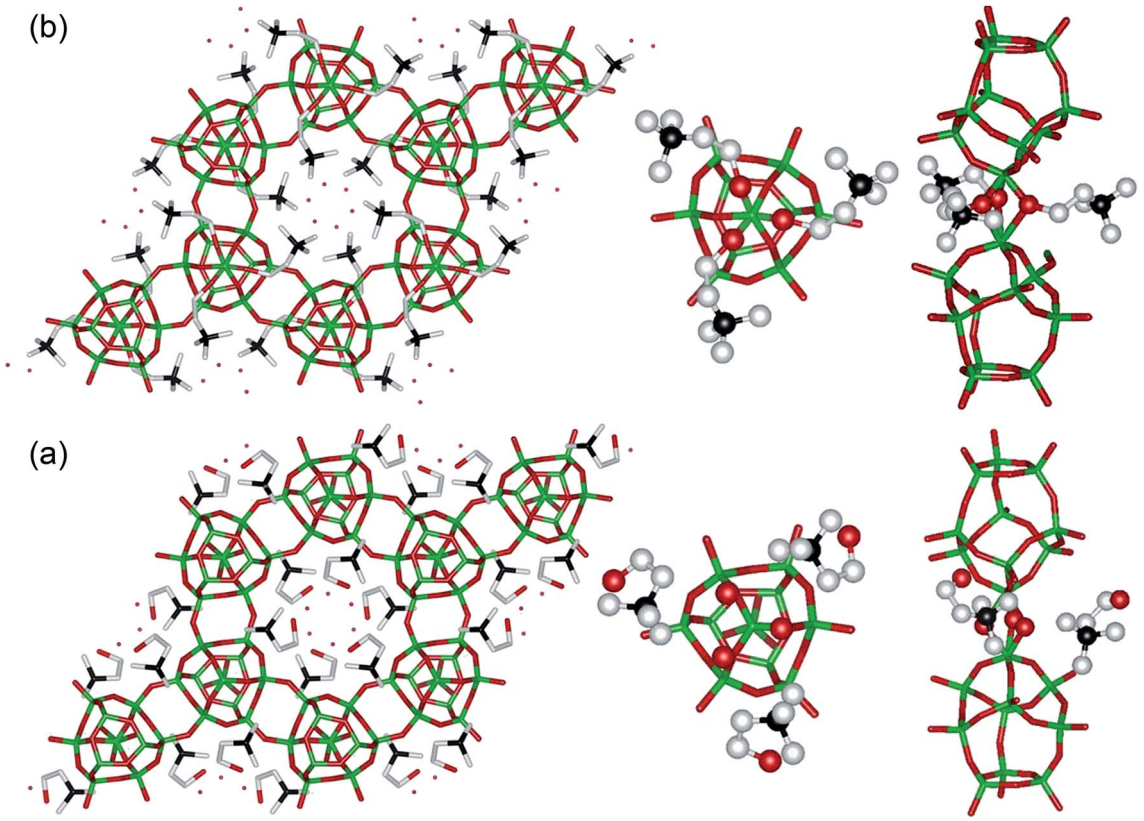

Fig. 2 As-made, hydrated (a) ECR-40C-Model A and (b) ECR-40C-Model B. Top view (left) of the 12-ring channel and top (middle) and side (right) views of its structural building unit. The $HTMA^+$ ions and framework O atoms bridging two $[3^14^65^6]$ bridging units of the MEI topology in ECR-40C-Model A are indicated using a ball-and-stick model, and the water O atoms are represented by dots. Color code: green, Al, P or Si atom; red, O; gray, C; black, N. H atoms are omitted for clarity.

former material. This prompted us to take much interest in the structure of ECR-40C.

Like the case for the as-made, hydrated ECR-40A, the synchrotron powder XRD pattern for as-made, hydrated ECR-40C was indexed according to a hexagonal unit cell with $P6_3$ space group. During the course of optimization of the locations and orientations of OSDA molecules in this material using the parallel tempering method implemented in the FOX program, however, two different types of $HTMA^+$ ions with a probability of approximately 3 : 2 have been continuously observed: one is the encapsulated species with one intramolecular C–H···O hydrogen bond as seen in as-made UZM-22 synthesized with the same OSDA, and the other is framework-bound ones like the $THMA^+$ ions in ECR-40A, denoted ECR-40C-Model A and ECR-40C-Model B, respectively.[11] Of unexpected interest is that both structure models derived based on these two types of $HTMA^+$ ions have been successfully refined against synchrotron powder XRD data (Fig. S2 and Tables S2–S5, ESI†). This implies that powder XRD cannot clearly discern between both models.

As shown in Fig. 2, the $HTMA^+$ ions in ECR-40C-Model A would adopt a *gauche* conformation stabilized by one intramolecular hydrogen bond between the O atom of its OH group and the hydrogens of carbon atoms linked to the charged nitrogen center. It is interesting to note here that the locations of $HTMA^+$ ions are quite similar to those of the same cations in the as-made form of aluminosilicate zeolite UZM-22.[25] We also found that an O atom in each of the three independent OH groups, which is not from OSDA molecules, is within covalent bond distance (1.74 and 1.94 Å) to the apex atoms of the two 13-hedral $[3^14^65^6]$ building units in the MEI topology. These two apex atoms are octahedral, because there are three bridging OH groups between them, as well as three O atoms linked to the T-atoms. This configuration prevents the violation of the Loewenstein's rule, the avoidance of tetrahedral Al–O–Al linkages,[26] which is energetically unfavorable to achieve during the hydrothermal synthesis of zeolites and related materials. The ^{27}Al MAS NMR data, as well as the variable-temperature IR results, supporting the presence of a pair of face-sharing AlO_6 octahedra consisting of such OH groups in ECR-40C-Model A will be given below.

On the other hand, ECR-40C-Model B shows that the O atom in each $HTMA^+$ ion bridges two apex Al atoms of the two $[3^14^65^6]$ building units located up and down along the *c*-axis, with Al–O bond lengths of 1.89 and 2.09 Å, respectively. Hence, these framework Al atoms are covalently bonded with six O atoms, because they are also bonded with another three framework O atoms linked to the P atoms within site T_1 in the $[3^14^65^6]$ building unit.[17] Although the structural analysis of as-made, hydrated ECR-40C has revealed that $HTMA^+$ ions could exist as two different types in ECR-40C, however, this did not allow us to

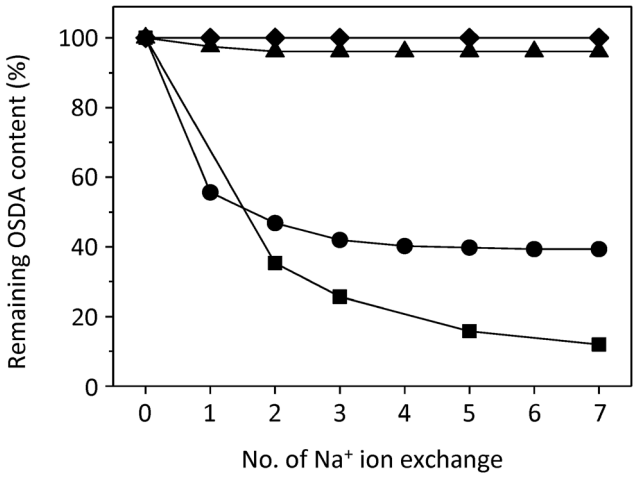

Fig. 3 Changes in the OSDA cation content as a function of the number of Na^+ ion exchange steps in as-made UZM-22 (■), PST-10C (▲), ECR-40C (●) and ECR-40A (◆). While the first three materials were synthesized with $HTMA^+$, the latter one was prepared in the presence of $THMA^+$. Each ion exchange was performed at 80 °C for 4 h using 1.0 M $NaNO_3$ solutions, and the remaining amount of OSDAs was measured by TGA/DTA.

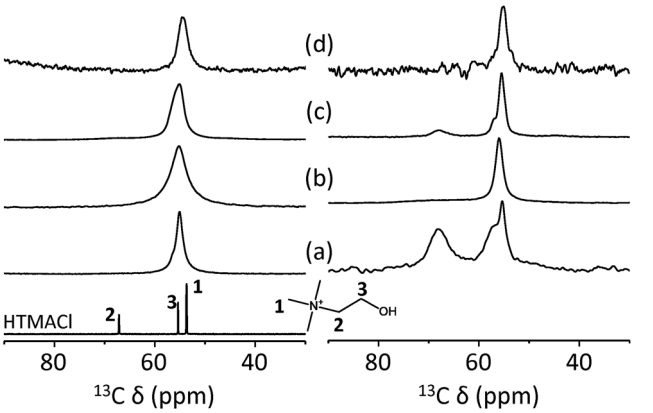

Fig. 4 ^{13}C MAS (left) and $^1H-^{13}C$ CP MAS (right) NMR spectra of the as-made form of (a) UZM-22, (b) PST-10C and (c) ECR-40C and (d) the seven-times Na^+-exchanged form of ECR-40C. The ^{13}C solution NMR spectrum of HTMACl in D_2O is also given for comparison.

unambiguously ascertain the simultaneous existence of both zeolite and FOMS domains in this inorganic–organic hybrid material. To obtain clearer evidence, therefore, we have used various additional characterization methods, the results of which will be given below.

We have also determined the structure of as-made, hydrated PST-10C, the GeAPO version of ECR-40C synthesized with the same OSDA (*i.e.*, $HTMA^+$) and 2 wt% (relative to alumina in the GeAPO gel) of the SAPO FOMS ECR-40A as seed crystals, using synchrotron powder XRD and Rietveld analyses. The substitution of Si by Ge leads to an increase (*ca.* 0.2 Å) in the unit cell edge along the *c*-axis, with the *a* cell edge almost constant (Table S1, ESI†). Unlike the case in ECR-40C, however, we were able to find no signs of the presence of the encapsulated $HTMA^+$ ions with one intramolecular hydrogen bond in PST-10C. As shown in Fig. S3 and Tables S6 and S7 (ESI†), all OSDA molecules are directly bonded to framework Al atoms. Therefore, PST-10C is really a pure FOMS, which can be further supported by the Na^+ ion exchange, and multinuclear MAS NMR and IR results given below. This is not unexpected because aluminogermanate zeolites are much rarer than aluminosilicate ones.[17]

Cation exchange and subsequent characterization

We next carried out ion exchange experiments using 1.0 M solutions of iodide salts of $THMA^+$, $BHDMA^+$ and $HTMA^+$ cations into calcined UZM-22 in order to check whether these OSDA species with different numbers of ethanol groups and thus different molecular sizes, used as OSDAs in the synthesis of ECR-40A, ECR-40B and ECR-40C or UZM-22, respectively, can enter into the 12-ring (6.9 × 6.9 Å) channels in the MEI structure. As shown in Fig. S4 (ESI†), the contents of all three organic cations including $THMA^+$, the largest OSDA among them, gradually increase with increasing the number of ion exchanges. This indicates that they can be introduced into or

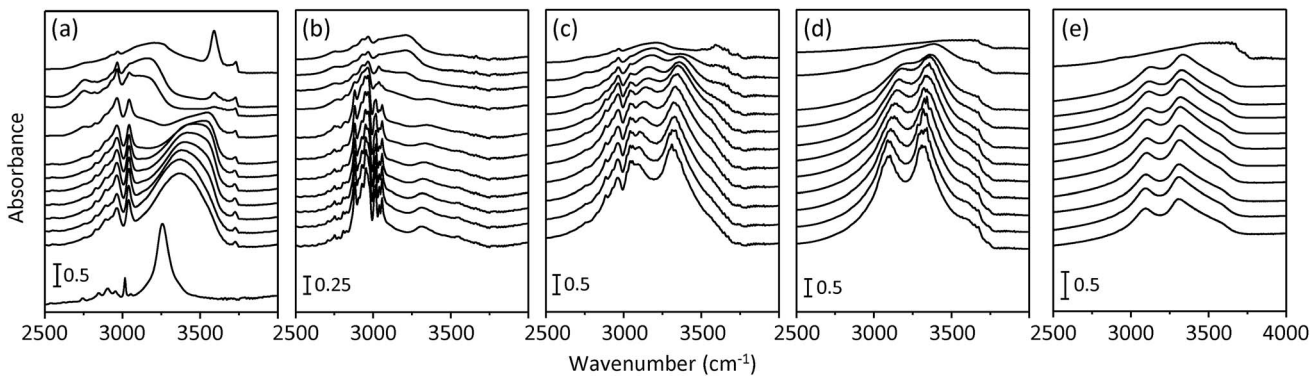

Fig. 5 IR spectra in the 2500–4000 cm^{-1} region of the as-made form of (a) UZM-22, (b) PST-10C and (c) ECR-40C, (d) the seven-times Na^+-exchanged form of ECR-40C and (e) boehmite recorded during *in situ* heating under vacuum to a residual pressure of 10^{-3} Torr at intervals of 50 °C. The bottom and top traces are the spectra measured at room temperature and 500 °C, respectively. For comparison, the room-temperature spectrum of HTMACl is given below that of as-made UZM-22.

extracted from the 12-ring channels in UZM-22 by ion exchange. However, if the ECR-40 family of molecular sieves are true FOMSs, the OSDA cations used in their synthesis should be covalently bonded to the inorganic framework. Since their extraction may not be possible by ion exchange, in consequence, this dynamic stoichiometric process is a simple but efficient tool for ascertaining the existence of the zeolite-like domain in FOMSs.

Fig. 3 shows changes in the OSDA cation content as a function of the number of Na^+ ion exchanges in the as-made form of UZM-22, PST-10C and ECR-40C, all of which were synthesized using $HTMA^+$. The organic variation in as-made ECR-40A is also given for comparison. After the seventh ion exchange, the $HTMA^+$ content in as-made UZM-22 decreases to *ca.* 10% of its original content. However, no detectable decrease in organic content is observed for both as-made PST-10C and ECR-40A even after the seventh ion exchange, revealing their pure FOMS nature. More interestingly, approximately 40% of the original $HTMA^+$ content in as-made ECR-40C were found to remain after the same number of Na^+ ion exchanges. This indicates that the proportion of its zeolite and FOMS domain is about 3 : 2, in excellent agreement with the structural characterization results described above.

Fig. 4 shows the ^{13}C MAS and ^{1}H–^{13}C CP MAS NMR spectra of the as-made forms of UZM-22, PST-10C and ECR-40C and the seven-times Na^+-exchanged form of ECR-40C, together with the ^{13}C solution NMR spectrum of HTMACl in D_2O. All the ^{13}C MAS NMR spectra are characterized by one resonance around 55 ppm, revealing that the two different CH_2 carbons of their $HTMA^+$ ions organic guest molecule are much less mobile than the CH_3 carbons. The same line shape is observed from the ^{1}H–^{13}C CP MAS NMR spectrum of as-made PST-10C, which confirms direct chemical bonding between the OSDA molecules and the inorganic framework in this member of GeAPO FOMSs. On the other hand, the ^{1}H–^{13}C CP MAS NMR spectra of as-made UZM-22 and ECR-40C exhibit two additional resonances around 57 and 68 ppm, revealing the presence of occluded OSDA, typical in zeolites and related microporous materials. In the case of as-made ECR-40C, the two low-field ^{13}C resonances disappear upon being Na^+-exchanged seven times. Since the resonance around 55 ppm is still detectable, however, the $HTMA^+$ ions remaining in seven-times Na^+-exchanged ECR-40C should be framework-bound ones. Therefore, it is again clear that ECR-40C contains both zeolite and FOMS domains.

Fig. 5 shows the variable-temperature IR spectra in the C–H and O–H stretching regions of the as-made form of UZM-22, PST-10C and ECR-40C, the seven-times Na^+-exchanged form of ECR-40C and boehmite (γ-AlOOH). For comparison, the room-temperature spectrum of HTMACl is also given in Fig. 5. The room-temperature IR spectrum of as-made UZM-22 shows a strong but much broader band around 3370 cm^{-1}, the wavenumber of which is higher by *ca.* 110 cm^{-1} than that (3258 cm^{-1}) of the hydrogen-bonded OH band observed in the IR spectrum of HTMACl. This band, which has been attributed to the OH group of the occluded $HTMA^+$ ion involved in intramolecular C–H···O hydrogen bonding,[16] becomes weaker with increasing the temperature to 300 °C, whereas another broad band around 3550 cm^{-1} assignable to the free OH group of the same organic cation appears. Interestingly, the room-temperature IR spectrum of as-made PST-10C gives a very weak O–H stretching band around 3310 cm^{-1}. Because there are many strong C–H stretching bands in the 2700–3100 cm^{-1} region, however, we can conclude that most, if not all, of the O atoms of $HTMA^+$ ions in as-made PST-10C have no hydrogens, but are involved in covalent bonding with framework Al atoms. This is in line with the Na^+ ion exchange results (Fig. 3), as well as with

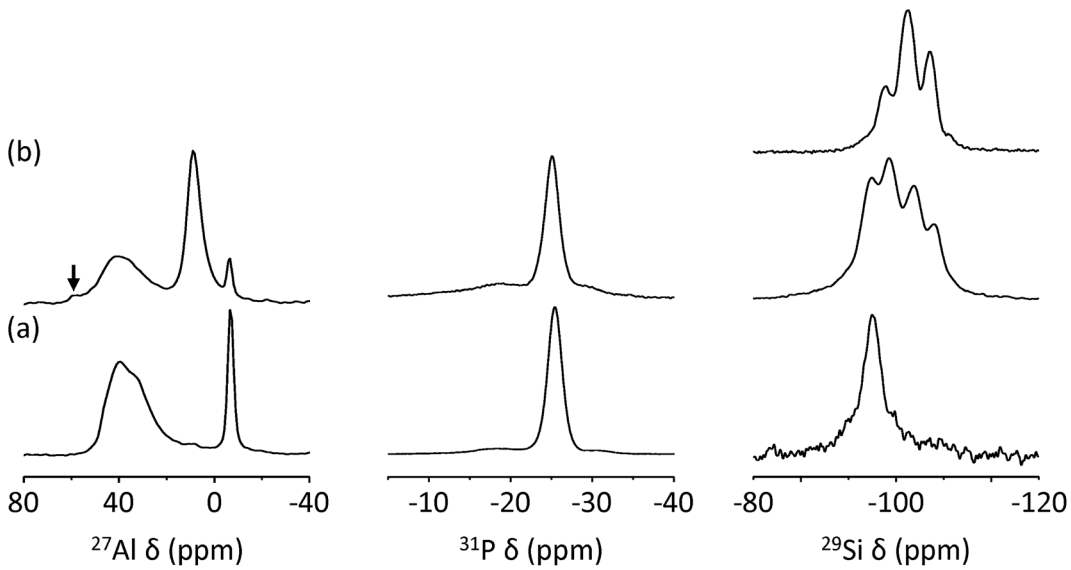

Fig. 6 ^{27}Al (left), ^{31}P MAS (middle) and ^{29}Si (right) MAS NMR spectra of as-made, dehydrated (a) ECR-40A and (b) ECR-40C. The ^{29}Si MAS NMR spectrum of as-made, dehydrated UZM-22 is given above that of as-made, dehydrated ECR-40C. The ^{27}Al resonance at 55 ppm assignable to tetrahedral Al in the zeolite domain is indicated with an arrow.

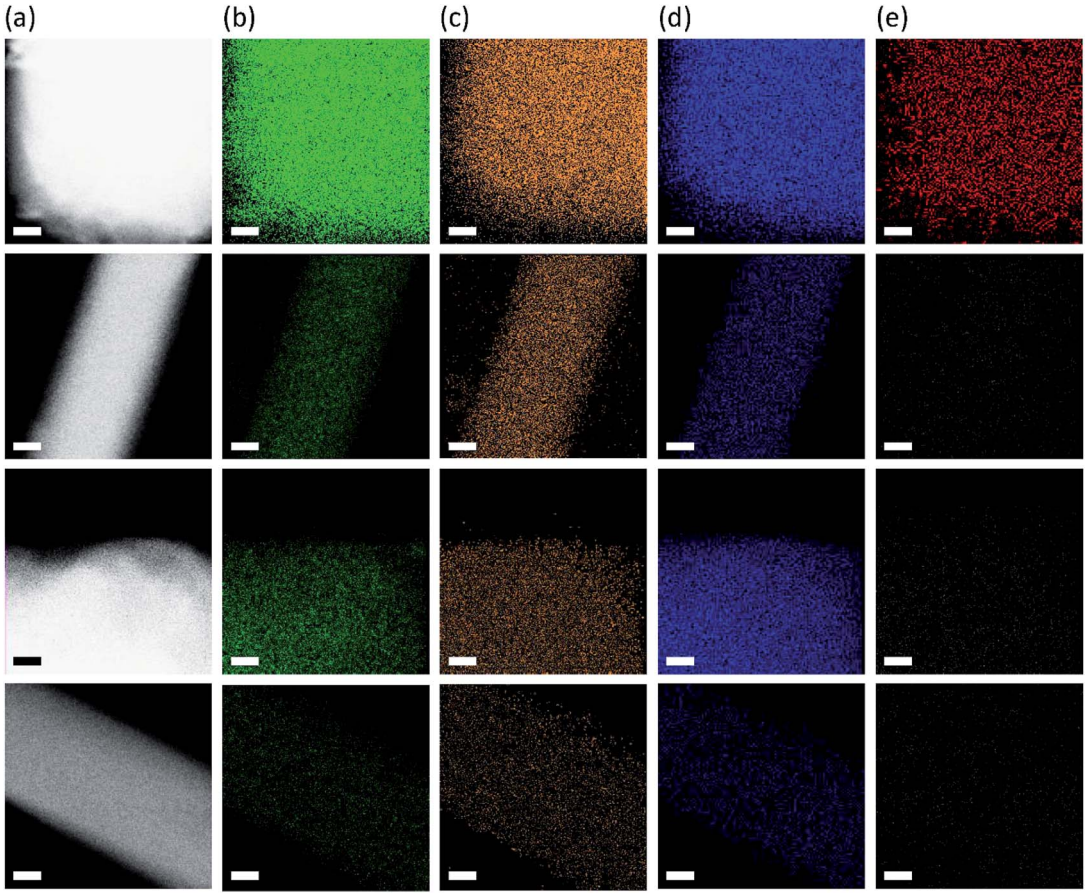

Fig. 7 (a) TEM and (b) Al, (c) P, (d) Si and (e) Na TEM elemental mapping images of the as-made (bottom two columns) and seven-times Na^+-exchanged (top two columns) forms of ECR-40A and ECR-40C. Scale bars, 20 nm.

its structure determined by powder XRD and Rietveld analyses (Fig. S3, ESI†).

Another interesting observation obtained from Fig. 5 is that unlike as-made UZM-22 and PST-10C, as-made ECR-40C shows two strong O–H stretching bands around 3310 and 3095 cm^{-1}. Both bands also show a fairly smaller increase in wavenumber with increasing temperature than that observed for the O–H stretching band from the $HTMA^+$ ions in as-made UZM-22. In particular, the lower-wavenumber band becomes more apparent after the seventh Na^+ ion exchange (*i.e.*, the extraction of occluded $HTMA^+$ ions). This suggests that the two strong O–H stretching bands from seven-times Na^+-exchanged ECR-40C cannot be due to $HTMA^+$ OH groups. It is worth noting that their wavenumbers are quite similar to the values of the two O–H stretching bands from γ-AlOOH. This topotactic precursor of γ-alumina exists in a hexagonal closed-packed arrangement of hydrogen-bonded oxides built up of edge-sharing $AlO_4(OH_2)$ or $AlO_3(OH)_3$ octahedral units.[27] Therefore, the IR data for seven-times Na^+-exchanged ECR-40C in Fig. 5 would correlate well with the structure of ECR-40C-Model A in Fig. 2: there are three independent OH groups, all of which are directly bonded to the apex atoms of 13-hedral $[3^1 4^6 5^6]$ building units.

Fig. 6 shows the ^{27}Al, ^{31}P and ^{29}Si MAS NMR spectra of as-made, dehydrated ECR-40A and ECR-40C. The ^{29}Si MAS NMR spectrum of as-made, dehydrated UZM-22 is also given for comparison. Dehydration was performed by heating under vacuum to a residual pressure of 10^{-3} Torr overnight at 200 °C, allowing us to ignore the water effects on the MAS NMR spectra in Fig. 6. While no noticeable differences in the line shape are found in the ^{31}P MAS NMR spectra of ECR-40A and ECR-40C, this is not the case of their ^{27}Al MAS NMR spectra. Both materials show two sharp ^{27}Al resonances around −9 and 9 ppm assignable to AlO_6 octahedra covalently bonded to OSDA molecules and to three independent OH groups, respectively,[11] as well as a broad and asymmetric ^{27}Al resonance around 40 ppm due to tetrahedral Al atoms in the SAPO framework.[28] However, the intensity of the former ^{27}Al resonance is considerably stronger for ECR-40A, a pure FOMS. As shown in Fig. 6, moreover, the intensity of the latter resonance is much stronger for ECR-40C. The existence of the zeolite domain in this material can be further supported by the appearance of a weak ^{27}Al resonance around 55 ppm, typical of tetrahedral Al in the zeolite framework.[28]

As recently reported,[10] the ^{29}Si MAS NMR spectrum of ECR-40A shows only one resonance around −94 ppm assignable to the $Si_3(2Si,2Al)$ species. However, the spectrum of ECR-40C is characterized by an additional three resonances around −98, −103 and −107 ppm, which is indicative of its higher Si content

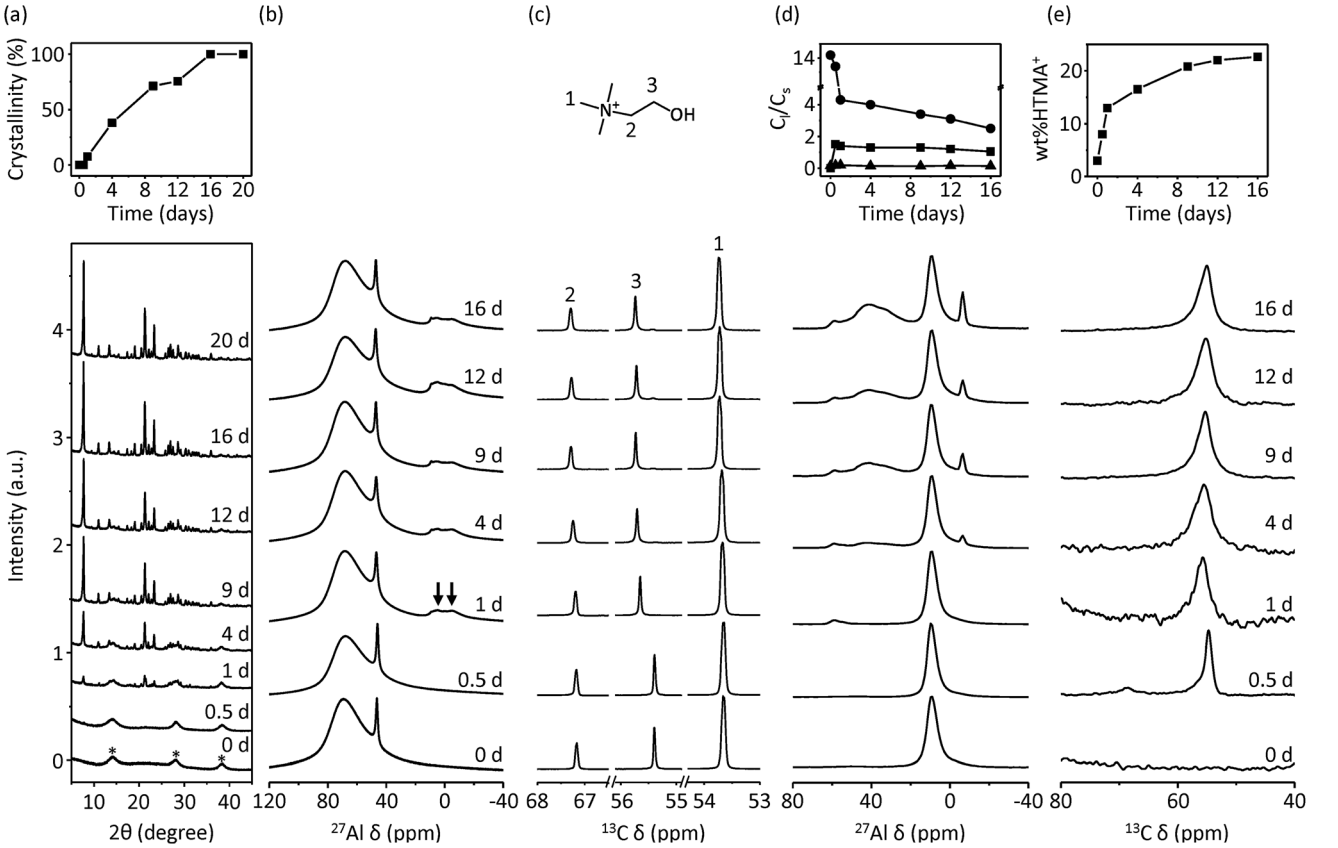

Fig. 8 Characterization of a series of mother-liquors and solid products separated after ECR-40C crystallization at 140 °C for different times. (a) Powder XRD patterns and (d) ^{27}Al and (e) ^{13}C MAS NMR spectra of solid product series. The X-ray peaks from pseudoboehmite, the alumina starting material, are marked by asterisks. To more clearly display changes in the resonance intensity, the amount of solid samples used in the MAS NMR experiments was kept constant. The relative crystallinities of solid products, the partition of Al (■), P (●) and Si (▲) between mother-liquors and solid products, and the organic contents of solid product series are also shown in panels (a), (d) and (e), respectively. (b) ^{27}Al and (c) ^{13}C NMR spectra of mother-liquor series. Two octahedral ^{27}Al resonances around 5 and −4 ppm are indicated with arrows. The assignment of each ^{13}C resonance for HTMA$^+$ is also shown in panel (c).

compared with ECR-40A. It is interesting to note here that their chemical shifts are quite similar to the values of the three major resonances appearing around −97, −102 and −107 ppm in the ^{29}Si MAS NMR spectrum of aluminosilicate zeolite UZM-22 with Si/Al = 4.7, as shown in Fig. 6. Our attempts to simulate the ^{29}Si MAS NMR spectrum of ECR-40C by combining the spectrum of ECR-40A with that of UZM-22 were not successful, probably because the T–O–T angle range for the four crystallographically different T-sites in the UZM-22 framework is not narrow enough to get into a single ^{29}Si resonance envelope.[16] Another reason may be that the T–O–T angles and ^{29}Si chemical shifts for each environment in a true solid solution should not be the same as those in their pure forms: there must be distortions and interactions due to the close proximity of both types of conformations.

Fig. 7 shows the TEM elemental mapping images of the as-made and seven-times Na$^+$-exchanged forms of ECR-40A and ECR-40C. These data reveal that the framework elements, (*i.e.*, Al, P and Si) are always homogeneously distributed throughout the crystals of all four materials. As expected, in addition, the Na$^+$ ions, which cannot be substituted for the framework-bound OSDAs in FOMS crystals, are hardly detectable from ECR-40A even after the seventh Na$^+$ ion exchange, consistent with the Na$^+$ ion exchange results in Fig. 3. As shown in Fig. 7, however, they are clearly visible from ECR-40C, the zeolite domain of which contain HTMA$^+$ acting both as a charge-compensating cation and as an OSDA, after the seventh Na$^+$ ion exchange. A more important observation is that the distribution of Na$^+$ ions in seven-times Na$^+$-exchanged ECR-40C is quite uniform throughout the crystals. Therefore, it is clear that ECR-40C is a new class of crystalline inorganic–organic hybrid materials different from FOMSs, that is, a solid solution of a zeolite and a FOMS.

Formation pathway for ECR-40C

To understand the formation pathway for this new class of solid solutions, we separated the mother-liquors and solid products as a function of crystallization time during the HTMA$^+$-mediated synthesis of ECR-40C and collected their multinuclear solution and solid-state NMR data, respectively. When the synthesis was performed under rotation (60 rpm) at 140 °C, it was finished after 16 days. However, the crystalline order detectable by powder XRD was already present after 1 day. As shown in Fig. 8, in addition, an Al–HTMA$^+$ complex in the liquid

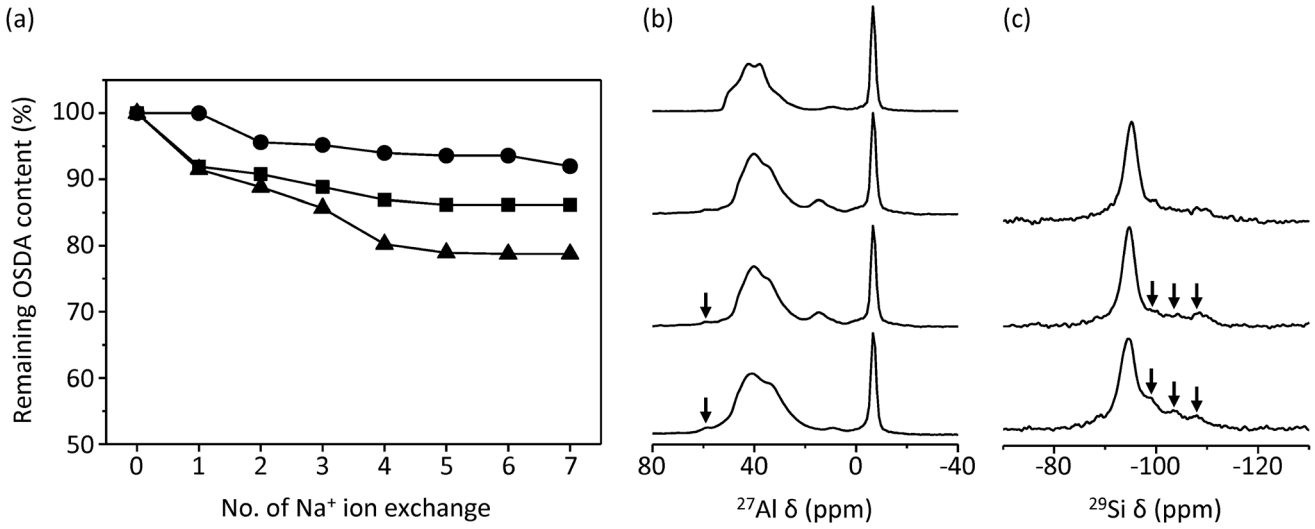

Fig. 9 Changes in the OSDA cation content (left) as a function of the number of Na^+ ion exchanges in as-made ECR-40B (■), ECR-40D (▲) and ECR-40E (●) and ^{27}Al (middle) and ^{29}Si (right) MAS NMR spectra of the dehydrated form of the corresponding materials (bottom to top). The ^{27}Al MAS NMR spectrum given above that of as-made, dehydrated ECR-40E was obtained from as-made, dehydrated PST-10C. One weak ^{27}Al resonance at 55 ppm and three weak ^{29}Si resonances around −98, −103 and −107 ppm assignable to tetrahedral Al and Si species in the zeolite domain, respectively, are indicated with arrows.

phase was also formed at that time,[11] as supported not only by two additional weak resonances around 5 and −4 ppm in the ^{27}Al NMR spectrum, but also by the change in ^{13}C chemical shift of a resonance at 55.4 ppm to 55.6 ppm that should correspond to the CH_2 carbon next to the OH group in $HTMA^+$ bonded to Al. This indicates that Al–$HTMA^+$ complex formation is not a critical factor governing the crystallization of ECR-40C at 140 °C until 1 day, unlike the $THMA^+$-mediated synthesis of ECR-40A at 160 °C.

The ^{27}Al MAS NMR spectra of the solid products separated after heating for 0 and 0.5 days exhibit no detectable tetrahedral Al species, suggesting that the UZM-22 seed crystals added were fully dissolved in the synthesis mixture. However, the spectrum of the solid product recovered after 1 day shows a new ^{27}Al resonance around 55 ppm assignable to the tetrahedral Al atoms in the aluminosilicate zeolite domain. In fact, the ^{29}Si MAS NMR spectrum of this solid gives three resonances around −98, −103 and −107 ppm (Fig. S5, ESI†), like those found in the ^{29}Si MAS NMR spectrum of UZM-22. Also, its ^{13}C MAS NMR spectrum shows signs of the $HTMA^+$ resonance with considerable mobility, unlike the OSDA molecules in ECR-40A. As shown in Fig. 8, on the other hand, the two ^{27}Al resonances appearing around 40 and −7 ppm, which are due to framework tetrahedral Al and octahedral Al atoms directly bonded to OSDAs in the SAPO FOMS domain, respectively, begin to be detectable from the solid product recovered after 4 days. Moreover, the ^{29}Si and ^{31}P MAS NMR spectra of this product show signs of the resonances around −94 and −26 ppm assignable to the Si_3(2Si,2Al) and P_1(4Al) species, respectively (Fig. S5, ESI†), in a manner similar to the case of ECR-40A synthesis.[10,11] The new ^{29}Si and ^{31}P resonances become stronger until ECR-40C crystallization is complete. Therefore, we can conclude that the formation of the zeolite domain is followed by that of the SAPO FOMS domain.

Fig. 9 shows the Na^+ ion exchange results for as-made ECR-40B, ECR-40D and ECR-40E, which were SAPO versions synthesized with $BHDMA^+$, BHMA, and BHEA, respectively, and the ^{27}Al and ^{29}Si MAS NMR spectra of their dehydrated form. The ^{27}Al MAS NMR spectrum of as-made, dehydrated GeAPO FOMS PST-10C is also given for comparison. Our recent synchrotron powder XRD and Rietveld analyses on the first two materials have revealed that both of them are in principle FOMSs.[11] As shown in Fig. 9, however, *ca.* 10 and 20% of their initial OSDA contents can be Na^+-exchanged, respectively, suggesting the presence of the zeolite domain. This can be further supported by the appearance of one weak ^{27}Al resonance around 55 ppm, absent in the ^{27}Al MAS NMR spectrum of PST-10C, and three weak ^{29}Si resonances in the chemical shift region higher than −95 ppm, all of which should be due to the aluminosilicate zeolite domain. Therefore, ECR-40B and ECR-40D would better be considered actually as solid solutions rather than as pure FOMSs, although with only a small proportion of the zeolite domain.

The overall characterization results of this work indicate that the proportion of the zeolite domain becomes larger with decreasing the number of OH groups in OSDAs, when alkanolammonium ions are used as OSDAs in the synthesis of ECR-40-type solid solutions. For example, $HTMA^+$ with one OH group cannot be more effective for Al–$OSDA^+$ complex formation and thus for FOMS crystallization than $THMA^+$ with three OH groups. In addition, neutral alkanolamines cannot form Al–$OSDA^+$ complexes more effectively than alkanolammonium cations. Apparently, the existence of such solid solutions suggests that the formation energetics of zeolites and FOMSs are not much different from each other. Therefore, we think that the synthesis of other families of zeolite–FOMS solid-solutions may also be possible.

Conclusions

The first solid-solution of a zeolite and a FOMS has been demonstrated. We have refined two models of the as-made, hydrated form of ECR-40C synthesized with $HTMA^+$ containing one OH group as an OSDA and a small amount (2 wt% of the alumina in the synthesis mixture) of aluminosilicate zeolite UZM-22 with the MEI topology as seeds, using synchrotron powder X-ray diffraction and Rietveld analyses. It was found that the $HTMA^+$ ions can exist in two different environments in ECR-40C with a probability of about 3 : 2. One is of occluded $HTMA^+$ ions present as the *gauche* conformer stabilized by one intramolecular C–H···O hydrogen bond, and the other is covalently framework-bound $HTMA^+$ cations. The coexistence of zeolite and FOMS domains in ECR-40C has been evidenced by the characterization results obtained using elemental and thermal analyses, Na^+ ion exchange, multinuclear MAS NMR, and variable-temperature IR. Furthermore, TEM elemental mapping reveals a homogeneous distribution of Na^+ ions exchanged into the as-made ECR-40C crystals. A thorough characterization of a series of mother-liquors and solid products separated as a function of time during the crystallization of ECR-40C clearly shows that zeolite domain formation takes precedence over FOMS domain formation. The proportion of the zeolite domain in such a new family of solid-solutions was found to differ notably according to the number of OH groups in OSDAs. In fact, we were also able to ascertain ECR-40B and ECR-40D, which were synthesized with $BHDMA^+$ and BHMA, respectively, as zeolite–FOMS solid solutions, although they are much closer to the FOMS end member. The overall results of this work strongly suggest that other families of zeolite–FOMS solid solutions can in principle exist. Apparently, the direct bonding of OSDAs with different types of functional groups to the zeolite framework can result in inorganic–organic hybrid materials with unusual properties. If such is the case, this would then allow us to broaden the application range of crystalline, microporous materials.

Acknowledgements

This work was supported by the National Creative Research Initiative Program (2012R1A3A-2048833) through the National Research Foundation of Korea. We thank Profs M. A. Camblor (ICMM) and X. Zou (Stockholm University) for helpful discussion and PAL for synchrotron diffraction beam time. PAL is supported by MSIP and POSTECH.

Notes and references

1 M. A. Camblor and S. B. Hong, in *Porous Materials*, ed. D. W. Bruce, D. O'Hare and R. I. Walton, Wiley, Chichester, 2011, p. 265.
2 M. Moliner, C. Martinez and A. Corma, *Angew. Chem., Int. Ed.*, 2015, **54**, 3560.
3 C. W. Jones, *Science*, 2003, **300**, 439.
4 C. W. Jones, K. Tsuji and M. E. Davis, *Nature*, 1998, **393**, 52.
5 H.-X. Li, M. A. Camblor and M. E. Davis, *Microporous Mater.*, 1994, **3**, 117.
6 K. Yamamoto, Y. Sakata, Y. Nohara, Y. Takahashi and T. Tatsumi, *Science*, 2003, **300**, 470.
7 G. Bellusi, A. Carati, E. D. Paola, R. Millini, W. O. Parker Jr, C. Rizzo and S. Zanardi, *Microporous Mesoporous Mater.*, 2008, **113**, 252.
8 G. Bellusi, E. Montanari, E. D. Paola, R. Millini, A. Carati, C. Rizzo, W. O. Parker Jr, M. Gemmi, E. Mugnaioli, U. Kolb and S. Zanardi, *Angew. Chem., Int. Ed.*, 2012, **51**, 666.
9 D. E. W. Vaughan, *US Pat.*, 5976491, 1999.
10 M. Afeworki, D. L. Dorset, G. J. Kennedy and K. G. Strohmaier, *Stud. Surf. Sci. Catal.*, 2004, **154**, 1274.
11 J. K. Lee, J. Shin, N. H. Ahn, A. Turrina, M. B. Park, Y. Byun, S. J. Cho, P. A. Wright and S. B. Hong, *Angew. Chem., Int. Ed.*, 2015, **54**, 11097.
12 D. S. Wragg, G. B. Hix and R. E. Morris, *J. Am. Chem. Soc.*, 1998, **120**, 6822.
13 L. Fang, L. Liu, Y. Yun, A. K. Inge, W. Wan, X. Zou and F. Gao, *Cryst. Growth Des.*, 2014, **14**, 5072.
14 S. Choi, J. H. Drese and C. W. Jones, *ChemSusChem*, 2009, **2**, 796.
15 M. A. Miller, J. G. Moscoso, S. C. Koster, M. G. Gatter and G. J. Lewis, *Stud. Surf. Sci. Catal.*, 2007, **170**, 347.
16 M. B. Park, S. J. Cho and S. B. Hong, *J. Am. Chem. Soc.*, 2011, **133**, 1917.
17 C. Baerlocher and L. B. McCusker, *Database of Zeolite Structures*, http://www.iza-structure.org/databases/.
18 R. W. Grosse-Kunstleve, L. B. McCusker and C. Baerlocher, *J. Appl. Crystallogr.*, 1999, **32**, 536.
19 C. Baerlocher, L. B. McCusker and L. Palatinus, *Z. Kristallogr.*, 2007, **222**, 47.
20 A. C. Larson and R. B. Von Dreele, *General Structure Analysis System (GSAS)*, Los Alamos National Laboratory, Los Alamos, New Mexico, 2000.
21 H. A. Rietveld, *J. Appl. Crystallogr.*, 1969, **2**, 65.
22 B. H. Toby, *J. Appl. Crystallogr.*, 2001, **34**, 210.
23 J. B. Hastings, W. Thomlinson and D. E. Cox, *J. Appl. Crystallogr.*, 1984, **17**, 85.
24 V. Favre-Nocolin and R. Černy, *J. Appl. Crystallogr.*, 2002, **35**, 734.
25 G. Wang, B. Marler, H. Gies, C. A. Fyfe, P. Sidhu, B. Yilmaz and U. Müller, *Microporous Mesoporous Mater.*, 2010, **132**, 43.
26 W. Loewenstein, *Am. Mineral.*, 1954, **39**, 92.
27 A. B. Kiss, G. Keresztury and L. Farkas, *Spectrochim. Acta, Part A*, 1980, **36**, 653.
28 G. Engelhardt and D. Michel, *High-Resolution Solid-State NMR of Silicates and Zeolites*, John Wiley & Sons, Chichester, 1987.

